ABUAD Journal of Engineering Research and Development (AJERD)
ISSN (online): 2645-2685; ISSN (print): 2756-6811

Volume 7, Issue 2, 39-50

Evaluation of Effective Interfacial Area in a Rotating Packed Bed Equipped with Dual Gas Inlets

Usman GARBA[1,2], David ROUZINEAU[2], Michel MEYER[2]

[1]*Faculty of Engineering and Environmental Design, Usmanu Danfodiyo University Sokoto, Nigeria*
usman.garba@udusok.edu.ng

[2]*Chemical Engineering Laboratory, University of Toulouse, CNRS, INPT, UPS, Toulouse, France*
usman.garba@udusok.edu.ng/david.rouzineau@ensiacet.fr;
michel.meyer@ensiacet.fr

Corresponding Author: usman.garba@udusok.edu.ng, +2347064436033
Date Submitted: 13/04/2024
Date Accepted: 29/06/2024
Date Published: 09/07/2024

Abstract: *This study investigates the effective interfacial area in a novel rotating packed bed (RPB) equipped with dual gas inlets instead of the conventional single-gas-inlet RPB. The aim is to enhance the mass transfer efficiency of gas-liquid contacting processes in RPBs by increasing the number of gas inlets to improve the spread of gas supply into the packing. The RPB is a promising gas-liquid contactor configuration known for its intensified mass transfer characteristics. However, the impact of additional gas inlets on the effective interfacial area of the packing remains unexplored. An experimental method assessed the interfacial area under varying operational conditions which include a liquid flow rate of 0.30-0.60 m^3/h, a gas flow rate of 100-300 Nm^3/h, and a rotation speed of 600-1000 rpm. At operating conditions covering the maximum rotation speed of 1400 rpm, gas flow and liquid flow rates of 300 Nm^3/h and 0.60 m^3/h respectively, the results showed that on average, 55 to 97% of the 2400m^2/m^3 specific packing area can be effectively utilized for gas-liquid mass transfer during separation operations using the RPB. Compared to results reported for single-gas-inlet RPBs using similar packings, the RPB with double gas inlet proved to provide higher utilization of the packing. By simply doubling the number of gas inlets, the findings provide valuable insights into optimizing RPB designs and operations which could enhance mass transfer efficiency for various chemical and environmental applications.*

Keywords*: Rotating Packed Bed, Dual Ga Inlets, Effective Interfacial Area, Structured Wire Mesh Packing, CO_2 Chemisorption.*

1. INTRODUCTION

A rotating packed bed (RPB) represents a process intensification apparatus leveraging centrifugal forces to enhance mixing and mass transfer, resulting in decreased equipment dimensions and reduced capital and operational expenses [1], [2]. The process intensification in RPBs is chiefly credited to the extensive specific surface area of the packings. Particularly in situations where size and space are restricted, RPBs present themselves as feasible alternatives for gas purification applications and various separation processes with higher mass transfer rates which is facilitated by increased interfacial areas,[3], [4]. RPBs, serving as process intensification equipment, find utility across a broad spectrum of practical applications such as absorption, adsorption, extraction, liquid contaminant removal, wastewater treatment, nanomaterial synthesis, rectification, and crude oil processing [1], [3], [5].

A key to simulating and designing gas-liquid contactors is mass transfer characteristics, including gas-side and liquid-side mass transfer coefficients, and effective interfacial area, which are measured via physical and chemical methods. The effective interfacial packing area (a_e) denotes the total contact surface area between gas and liquid phases in a two-phase flow system and is directly tied to the nature of the packing [3]. Therefore, in RPBs, the effective mass transfer area is a component of the interfacial packing area in contact with gas and liquid. Generally, for packing materials with relatively low static holdup, similar to most RPBs where packing sizes are small, the wetted area can be assumed to equate to the interfacial area.

Previous studies on conventional packed separation columns (CPSCs) generally indicated that enhancing specific areas and critical surface tension of the packing could enhance mass transfer efficiency. However, experimental outcomes suggest that in RPBs, the relationship between mass transfer and the specific surface area of the packing likely differ from that in CPSCs [3]. In their study, using RPBs of varying rotor sizes, Tian *et al.* [4] reported that the packing radius is the dominant factor that affects the value of the effective interfacial area while the liquid flow rate has the least influence. Invariably, the study showed that the axial packing height has little influence on the effective specific area in RPBs. Various methodologies have been suggested to determine mass transfer characteristics based on physical or chemical

principles. Literature indicates that effective surface area data for RPBs and other packed separation columns are often obtained using methods that involve measuring CO_2 absorption in NaOH solutions [6]. Thus, the most widely accepted and employed approach for evaluating mass transfer characteristics in RPBs involves chemically absorbing carbon dioxide gas into caustic soda [7]. Commonly utilized caustic solutions for CO_2 absorption include NaOH, KOH, and amines like MEA and piperazine. However, diverse physical and chemical test systems or approaches are employed to measure the effective interfacial area of packings. A review by Hegely et al. [7] identified several methods for determining the gas-liquid interfacial area in packed separation columns, encompassing chemical absorption, pure liquid vaporization, physical absorption, tomography, colorimetry, and packing sublimation. Factors contributing to high experimental values of a_e in RPBs, as listed by the authors, include the liquid spread in the azimuthal direction due to Coriolis force, low minimum wetting flow rate, low static holdup, low number of liquid-blocked passages, and good initial liquid distribution. Consequently, experimental values of the interfacial area to packing area ratio in RPBs tend to surpass those predicted by the commonly used Onda correlation. Notably, this ratio is higher in RPBs than in conventional gravity-flow packed beds.

In systems with fast or intermediate reaction regimes and established kinetics, where the absorption rate hinges on interfacial area, specific areas are measured using chemical absorption. Typically, highly pure solutes in the gas phase are employed to eliminate gas-side mass transfer resistances. Solute gases are often diluted with standard air as a carrier gas. A compilation of the effective interfacial area to total packing area ratio, also known as packing utilization factor or effective gas-liquid contacting efficiency ($\frac{a_e}{a_t}$) reported by Luo *et al.* [8], indicated that the total effective interfacial area for mass transfer, inclusive of liquid droplets, films, and other liquid flow patterns, is smaller than the total packing area, implying that the packing in RPBs is not constantly wetted by the liquid in the rotor. Literature indicated that the packing utilization factor in RPBs can reach as high as 98% (Table 2).

Given the intricate nature of liquid flow in RPBs, reliable data on the effective mass transfer area of the packing are imperative. Several researchers ([4], [9]) recommend the chemical absorption of CO_2 into NaOH solution as the standard test system for measuring the effective mass transfer area of packings. Consequently, several authors have employed the chemisorption of CO_2 with NaOH to estimate the effective mass transfer interfacial area in RPB packings ([8], [10], [11]). Utilizing the CO_2-NaOH system offers several advantages, including well-documented primary data on the reaction kinetics and physical properties of the system, ease of operation, and negligible error margin in estimating gas-phase mass transfer resistance due to the predominance of liquid-phase mass transfer control [9].

RPB mass transfer characteristics such as the effective interfacial area, and gas and liquid mass transfer coefficients were reported in several previous publications [3], [4], [8], [12], [13]. Many studies have been published on the effective interfacial area of RPB packings. To measure the actual effective gas-liquid interfacial area in the packing of an RPB, Yang *et al.* [11] installed a sampling tube close to the rotor. They collected the liquid flowing directly from the packing. The study reported that the space between the outer part of the packing and the rotor wall (the cavity zone) contributed an average of 13–25% of the total mass transfer of an RPB. To improve the mechanical strength and repeatability of stainless steel wire mesh packing, Luo et al. [8] designed and constructed an innovative structured stainless steel wire mesh packing equipped with twin ring baffles installed separately at the upper and the lower edge of the rotor. The effective interfacial area of the packings increased with increased gas flow rate, liquid flow rate, and rotational speed under the experimental conditions. On the contrary, Tian et al.[4] measured the effective interfacial area of three RPBs of varying rotor diameters under different operating conditions and reported that the rotation speed and the liquid flow rate were the major factors affecting the effective interfacial area while the influence of the gas flow rate was minimal. The impact of increasing the number of liquids inlet has been shown to greatly improve gas-liquid mass-transfer performance in RPBs [14], [15]. However, even as the chemical chemisorption of CO_2 in NaOH solution to measure the effective interfacial area of RPBs equipped stainless steel wire mesh packing has been widely researched [16], to the best of our knowledge, the influence of increasing the number of gas inlets on the mass transfer of RPBs is yet to be investigated. In this study, a standard RPB, R500, which is equipped with dual gas inlets is utilized to investigate the influence of the multiple gas inlets on the mass transfer efficiency.

2. EXPERIMENTAL SETUP AND METHODOLOGY

2.1 Interfacial Area Calculation

The chemical reaction between NaOH and CO_2, with NaOH in excess, is represented as follows:

$$NaOH_{(aq)} + CO_{2_{(g)}} \rightarrow Na_2CO_{3_{(aq)}} + H_2O_{(l)} \quad (1)$$

The dissolution of gaseous CO_2 into a 0.1M NaOH solution, a physical process, is described as:

$$CO_{2(g)} \leftrightarrow CO_{2(l)} \quad (2)$$

The rate-determining step is expressed as:

$$CO_{2(l)} + OH^- \overset{k_{OH-}}{\longleftrightarrow} HCO_3^- \quad (3)$$

Followed by an instantaneous proton transfer reaction:

$$HCO_3^- + OH^- \leftrightarrow CO_3^{2-} + H_2 \quad (4)$$

The method for calculating the interfacial area under different operating conditions is outlined thus:
The concentrations of OH^- and CO_3^{2-} within an aqueous NaOH sample of volume, V_{sample} are given by:

$$[OH^-] = \frac{[HCl]*V_{eq,1} - [CO_3^{2-}]*V_{sample}}{V_{sample}} \quad (5)$$

While,

$$[CO_3^{2-}] = \frac{(V_{eq,1} - V_{eq,2})*[HCl]}{V_{sample}} \quad (6)$$

$V_{eq,1}$ and $V_{eq,2}$ are the equivalent points of the titration obtained from the titration curve as displayed by an automatic potentiometric titrator. In the absorption of CO_2 in RPBs, a liquid-phase mass transfer process controls the rate, which is second-order. Hence, the overall reaction rate is expressed as the absorption rate of CO_2:

$$r_{CO_2} = k_2 C_{CO_2} C_{NaOH} \quad (7)$$

Here, k_2 represents the reaction rate constant.
Considering a material balance across the RPB, as depicted in Figure 1, the gas-liquid flux N_A over a differential radial distance, dr, is given by:

$$\frac{dG(r)}{dV} = N_A \quad (8)$$

Where G represents the amount of gas passing through the differential volume of the RPB in moles/m^2.hr. Thus, the rate of gas mass transfer to the liquid is given by:

$$\frac{d}{dV}G = K_G * a_e * (y - y^*) \quad (9)$$

K_G is the overall gas-side mass transfer coefficient while y and y^* are the molar concentrations of the gas in the bulk of the liquid and at equilibrium respectively.
Figure 1(a) shows a sectional schematic diagram of an RPB for taking a mass balance.

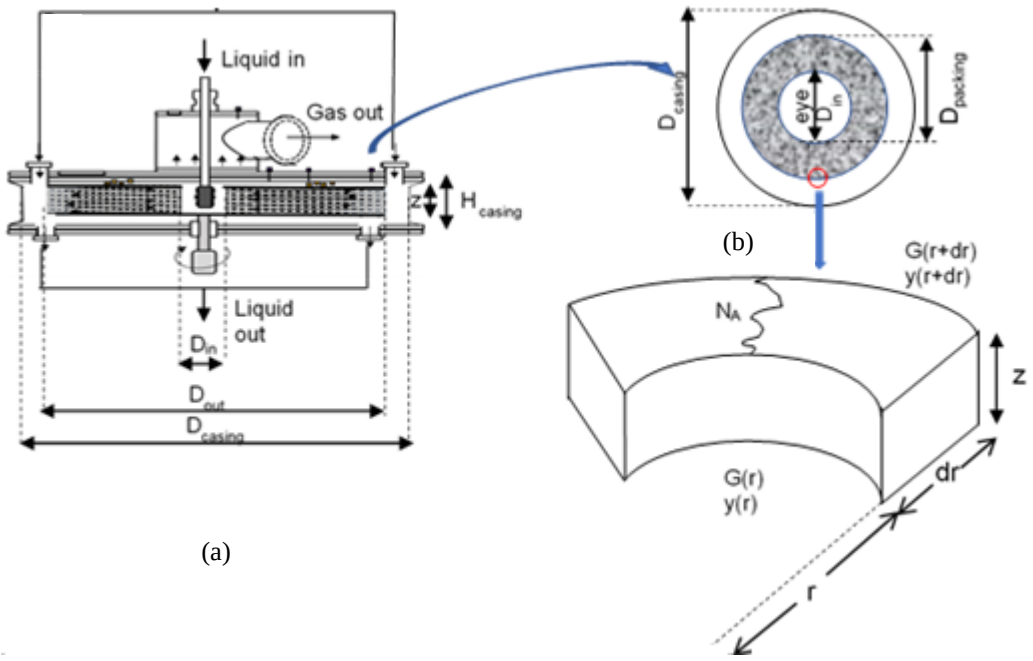

Figure 1 Schematic diagram of mass balance of an RPB packing

In Figure 1 (a), the outer diameter (D_{out}) of the packing is much larger than the inner diameter (D_{in}) to ensure the maximum liquid jet impact on the inner walls of the packing and to enable an optimum counter-current gas-liquid interaction within the radial length of the packing.

From Figure 1b, which shows a section of the packing of internal and external diameter, D_{in} and $D_{packing}$ respectively, the differential volume of the packing, dv, of axial height z can be expressed as:

$$dV = 2\pi rz * dr \tag{10}$$

Where r and z represent the inner radius and axial height of the packing, respectively.
Combining the equations yields:

$$\frac{d}{2\pi rzdr}\frac{Gy_{CO_2}P}{RT} = E * k_L * a_e * \left(C^*_{CO_2} - C_{CO_2}\right) \tag{11}$$

Where, E represents the enhancement factor, and k_L is the liquid-side mass transfer coefficient, C_{CO_2} and $C^*_{CO_2}$ are respectively, the CO_2 concentration of the liquid phase, and the CO_2 equilibrium concentration of the liquid phase relative to the gas phase measured in kmol/m^3.
Considering the conditions in the liquid, with excess NaOH,

$$C^{eq}_{CO_2} \sim 0 \tag{12}$$

$$C^{eq}_{CO_2} \ll C^*_{CO_2} \tag{13}$$

$$\frac{d}{2\pi rzdr}\frac{Gy_{CO_2}P}{RT} = E * k_L * a_e * \frac{y_{CO_2}\cdot P}{H_e} \tag{14}$$

Thus, rearranging Equation (11),

Rearranging Equation (12),

$$\frac{G}{RT} * \frac{dy_{CO_2}}{y_{CO_2}} = \frac{E\cdot k_L\cdot a\cdot h_P\cdot 2\pi}{H_e} * rdr \tag{15}$$

Thus,

$$\frac{G}{RT} * \left(lny_{CO_2,out} - lny_{CO_2,in}\right) = \frac{E\cdot k_L\cdot a_e\cdot z\cdot \cancel{2}\pi}{H_e(T)} * \left(\frac{r^2_{out}}{\cancel{2}} - \frac{r^2_{in}}{\cancel{2}}\right) \tag{16}$$

Introducing a constant A:

$$A = \frac{E\cdot k_L * z * \pi}{H_e(T)} * (r^2_{out} - r^2_{in}) \tag{17}$$

Where E, the enhancement factor expressed as:

$$E = \frac{\sqrt{k_r * D^L_{CO_2} * C^o_{OH^-}}}{k_L} \tag{18}$$

Substituting Equation (18) in Equation (17),

$$A = \frac{z*\pi}{H_e(T)} * \sqrt{k_r * D^L_{CO_2} * C^o_{OH^-}} * (r^2_{out} - r^2_{in}) \tag{19}$$

Where k_r is the rate constant of the pseudo-first-order reaction in m^3/kmol·s and its relationship with temperature and electrolyte concentration is:

$$k_r = 10^{\left(11.895 - \frac{2382}{T}\right)} * 10^{(0.221*I - 0.016\times I^2)} \tag{20}$$

Additionally, $D^L_{CO_2}$ denotes the diffusion coefficient expressed in m^2/s:

$$D^L_{CO_2} = 10^{\left(-8.1764 + \frac{712.52}{T} - \frac{259100}{T^2}\right)} \tag{21}$$

The Pohorecki and Moniuk model is chosen for calculating the kinetics of the reaction between CO_2 and OH^- ions in aqueous electrolyte solutions. The model is selected based on the recommendations of Sheng et al. [9] on standard methods for measuring mass-transfer characteristics in packed absorption columns and the authors' analysis concerning various models for measuring a_e in RPBs which showed that the values calculated from the Pohorecki and Moniuk model align closely with experimentally measured values as reported by many authors ([13],[19]). Consequently, the Henry constant, $H_e(T)$ in Pa·m^3/mol is expressed as:

$$H_e(T) = 10^{(9.1229 - 0.059044\times T + 0.000078857\times T^2)} * 10^{-h*I} \tag{22}$$

Where T represents the absolute temperature in K, and I denote the ionic strength in kmol/m^3, represented as:

$$I = \frac{1}{2} * \left(C_{Na^+} * z^2_{Na^+} + C_{OH^-} * z^2_{OH^-}\right) = 1 \tag{23}$$

Where z is the valence of the ions and h is the contribution of the cations, anions, and gas in the correlation, given in Equation (23), expressed in m^3/kmol.

$$h = h_+ + h_- + h_G = 0.091 + 0.066 + -0.000405263 * T - 0.00913158 \quad (24)$$

Thus, the effective interfacial area can be determined from:

$$a_e = \frac{G}{A \cdot RT} * \left(lny_{CO_2,out} - lny_{CO_2,in}\right) \quad (25)$$

2.2 Experimental Setup

A novel pilot-scale RPB (Prospin Poland, Model R500), featuring dual gas inlets situated at opposing ends of the upper rotor section, was utilized. Figure 2 illustrates a schematic representation of the RPB, as depicted in Garba *et al.* [17], while Table 1 outlines its specifications and the characteristics of the doughnut-shaped packing. Gas was directed inward from the outer periphery of the packing via pressure-driven force, whereas liquid concurrently flowed outward, dispersed by a central liquid distributor located at the core of the packing. This liquid distributor, comprising a full-jet single central design, featured an array of small holes, each with a diameter of 1.5mm, positioned in eight equidistant zones along the circumference of a pipe for optimal liquid dispersion.

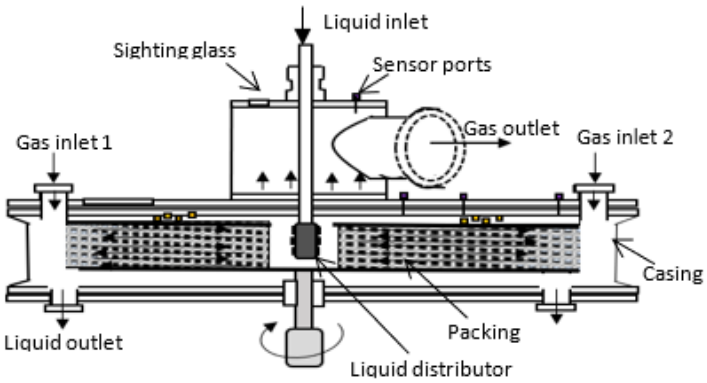

Figure 2: Schematic of a countercurrent flow RPB with dual gas inlets [17]

As the liquid distributor disperses liquid along the inner circumference of the packing, it traverses radially through the packing material. The discharged liquid accumulates at the base of the casing before exiting through two liquid outlets positioned at the bottom of the casing. Consequently, for the monitoring and regulation of the liquid level within the RPB, a hydraulic guard comprising a transparent, flexible spiral hose is employed to connect these liquid outlets to a storage tank. Additionally, two sighting glasses are affixed to the gas outlet flange to facilitate visual inspections of the rotor's center, where liquid entrainment may initiate due to reduced centrifugal force. Thus, ensuring the concurrent contact of gas and liquid completes the mass transfer process. Subsequently, the gas is expelled through the gas outlet, while the liquid is gathered along the casing walls and discharged via the two liquid outlets located at the base of the RPB.

Table 1: Main characteristics of the RPB500 and the packing

RPB	
Description	Pilot-scale, countercurrent with two gas inlets (2 x DN120)
Manufacturer	ProCeller, Poland, and supplied by Prospin, Poland
Inner rotor diameter, m	0.16
Outer rotor diameter, m	0.50
Outer casing diameter, m	0.65
Rotor height, m	0.04
Packing	
Type	Stainless-steel wire mesh
Manufacturer	ProCeller, Poland, and supplied by Prospin, Poland
Porosity	0.86
Packing area, m^2/m^3	2500
Axial height, m	0.04

Figure 3 depicts the schematic diagram of the experimental setup. The liquid was stored in a 0.6 m^3 reservoir tank. A second tank identical to the feed tank served as a drain for liquid disposal post-use. Typically, the reservoir tank was maintained at 60-70% capacity. To ensure uniformity of the mixture in the tank, an electric stirrer was installed. All ductwork was constructed from polypropylene, given the absence of corrosive materials. Liquid transfer from the tanks was facilitated by a magnetic drive pump (Iwaki, model MDG-R15P), featuring a size of 15:5.5 ml/revolution, a maximum

flow rate of 0.84m^3/h, and a maximum operational viscosity allowance of 30 mPa.s within a temperature range of 0 – 40°C. The pump was also used to circulate the liquid between the two tanks to ensure proper mixing before the commencement of each experimental run. By utilizing a three-way valve system, the solution was circulated between the RPB500, and the two tanks, enabling the flexible routing of the solution.

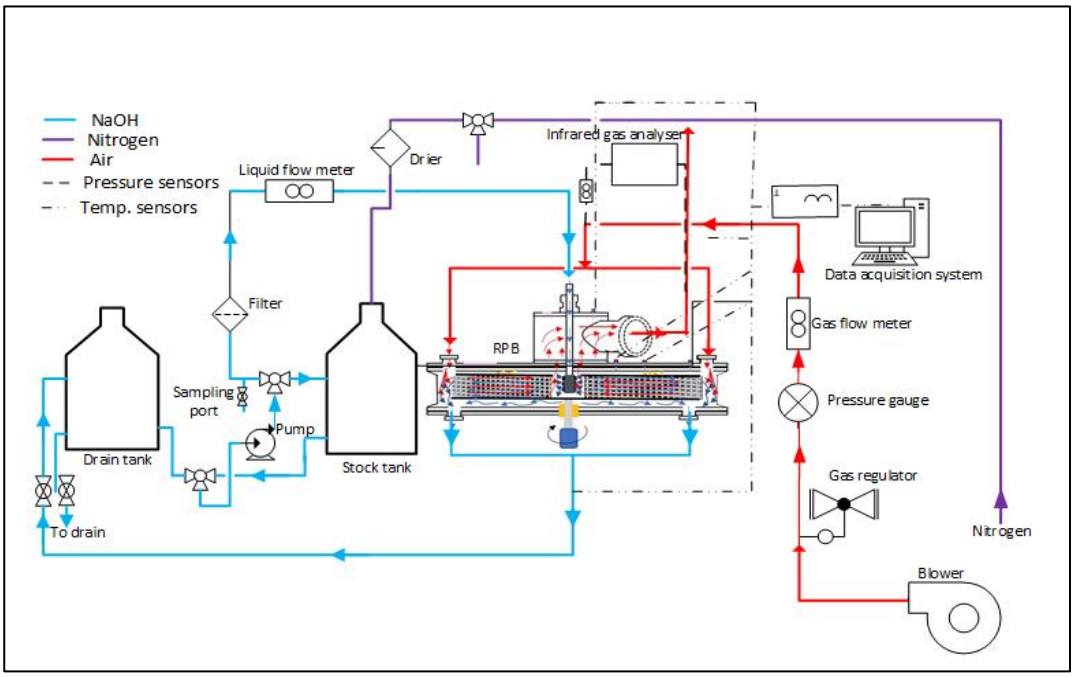

Figure 3 Experimental setup for measuring effective interfacial area in RPB500

2.3 Preparation and Storage of NaOH Solution

The NaOH solution utilized for the chemical absorption of CO_2 was derived from the precipitation of NaOH solid in deionized water. To fill the sump tank to approximately 70% of its capacity, a 0.1M NaOH solution totalling 0.5 m^3 was prepared. This involved dissolving 4.024kg of liquid NaOH (50/50 w/w) sourced from Gaches Chimie, France, in water to achieve the desired solution concentration. Subsequently, the sump tank underwent nitrogen purging from the laboratory mains supply to prevent the reaction of CO_2 naturally present in the air and to forestall carbonate formation. Furthermore, to shield the aqueous solvent supply tank from atmospheric pollutants, a 3-compartment filtration system was implemented, as illustrated in Figure 4. This system featured two filters containing silica gel to remove humidity and one filter containing soda pellets to isolate the tank from atmospheric CO_2. Consequently, while the solute load of the solvent was deemed negligible, it was still measured for verification purposes.

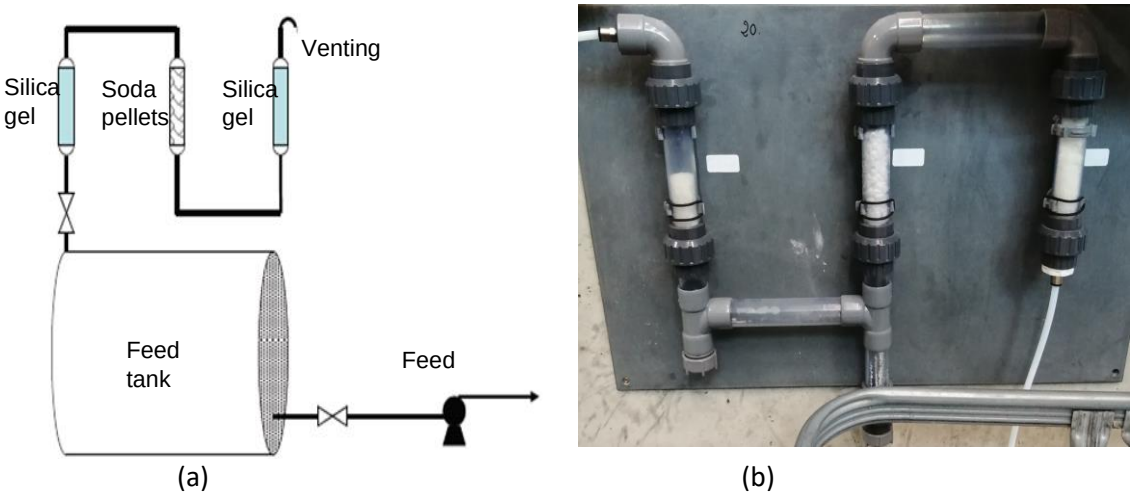

Figure 4: A 3-compartment filtration system for filtering humidity isolating the solvent tank from atmospheric CO_2 showing (a) a schematic diagram and (b) a picture of the set-up

2.4 Liquid Sampling Mechanism

For liquid sampling, the sampling port shown in Figure 5 which was regulated by a ball valve was installed at the liquid inlet to the storage tank. Before sampling, the liquid was thoroughly homogenized by recirculating it using the pump at a

high flow rate for approximately 30 minutes. To collect a sample of the liquid for analysis, a 5 x 10^{-5} m^3 sampling bottle was used. The sampling bottle, cleaned and dried beforehand, was rinsed twice with the sample to flush the sampling hose and rinse the bottle. Subsequently, a sample of approximately 4 x 10^{-5} m^3 from the well-mixed sample was extracted for analysis.

Figure 5: Liquid sampling port

2.5 Liquid Sample Analysis: Titration Procedure

To analyse the liquid samples, an automated potentiometric technique was employed. This method involves conducting acid-base titrations, precipitation reactions, and reduction-oxidation titrations with high-power magnetic stirring in an automated fashion. Automatic potentiometric titrators typically handle reagent injection, equivalence point determination, and automatic concentration calculations, and can detect multiple equivalence points. In this study, an automatic potentiometric titrator (Eco Titrator, Metrohm AG, Switzerland, model: 2.1008.0010) was utilized for liquid sample analysis. The concentration of NaOH and Na_2CO_3 in the collected liquid samples was determined using a 0.1M HCl solution for titration.

Additionally, the NaOH titration provided concentrations of OH^- and CO_3^{2-} with the OH^- coming from the titrator. These concentrations are crucial for estimating reaction kinetics and the Henry constant, while the CO_3^{2-} content indicates the need for solution renewal. Solution renewal occurred when CO_3^{2-}<0.02-0.03 mol^{-1} in 0.1N of the solutions.

2.6 Gas Supply, Distribution, and Analysis

Ambient airflow, powered by a single-stage side channel blower (BUTSCH SAMOS, SB 0430 D0), was employed for gas supply. The blower operates without oil lubrication, ensuring delivery of air free from compressor-induced impurities or contaminants, with a nominal pumping speed of 500 m3/h and a maximum differential pressure of 260 mbar. The airflow was directed from the blower to the RPB through a series connection of polyvinyl chloride (PVC) hoses, with a diameter of 0.569m, comprising a combination of spiral, clear flexible, and non-flexible wall-mounted hoses. While liquid flows radially outwards from the liquid distributor due to centrifugal acceleration, gas flows radially outwards through the packing due to pressure difference. Consequently, the gas enters the periphery of the packing and flows radially outwards through it. After counter-current contact with the liquid, the gas exits through the gas outlet at the top of the RPB and is ventilated to the atmosphere without pre-treatment, as the exit gas did not contain toxic gases in both experiments.

The gas outlet is equipped with a mechanism for gas exit and for trapping and collecting entrained liquid. Therefore, a hydrocyclone was designed, fabricated, and connected to the gas outlet to facilitate liquid collection. An infrared carbon dioxide analyser (Fisher Rosemount Analytical, NGA 2000 series, Model: MLT1.2IR-UV), with an accuracy of ±8%, was utilized to detect CO_2 concentrations at the gas inlet and outlet of the RPB. Gas analysis commenced by switching on the analyser, performing internal automatic calibration with nitrogen gas, setting the device to zero, and then connecting it to the gas supply. Inlet CO_2 concentration, subsequent outlet CO_2 concentrations, and corresponding temperatures during experimental runs were directly read from the gas analyser.

2.7 Experimental Procedure

The operational parameters employed ranged from an ambient airflow rate of 100-300 Nm^3/h, an aqueous 0.1M NaOH flow rate of 0.30-0.60 m^3/h, and a rotation speed of 600-1000 rpm. The minimum rotational speed was determined based on the liquid load and gas capacity factor to prevent liquid entrainment towards the gas outlet during operations. Initially, the rotational speed was set at its maximum value, 1000 rpm, and then gradually reduced in steps to 100 rpm. The effective interfacial area of the packing was determined by measuring CO_2 concentration at the inlet and outlet of the RPB for each experimental run after reaching a stabilization point.

3. RESULTS AND DISCUSSION

3.1 Time to Attain Steady State

Due to the system's sensitivity to both the RPB operating parameters and ambient conditions, the time required for the system to stabilize and reach a reasonably representative steady state was determined at the beginning of each experimental run. The system was set to moderate liquid and gas flow rates, along with rotation speeds, and allowed to operate. Gas analyser readings were recorded every 5 minutes until a stable reading was obtained. Figure 6 illustrates the results. Figure 6 illustrates the variation in the concentration of CO_2 for about 1 hour. At time zero, the concentration of the CO2 was 528 ppm for gas flow rate and rotation speeds of 100 Nm^3/h and 1000 rpm respectively. In the first 5 minutes, a rapid decrease in the concentration of CO_2 occurred, indicating a fast initial reaction rate. Subsequently, the rate of change for both the CO_2 began to slow between 10 and 40 minutes suggesting the system was approaching a steady state. The concentration curve flattened out after about 45 minutes, indicating that the system had reached a steady state. From 45 minutes onwards, there was no significant change in the concentration signifying that the steady state was attained. The trend was similar for a higher gas flow rate of 200 Nm^3/h and a lower rotation speed of 600 rpm where the concentration was initially at 408 ppm, decreased rapidly in the first 5 minutes with the steady state attained after about 40 minutes.

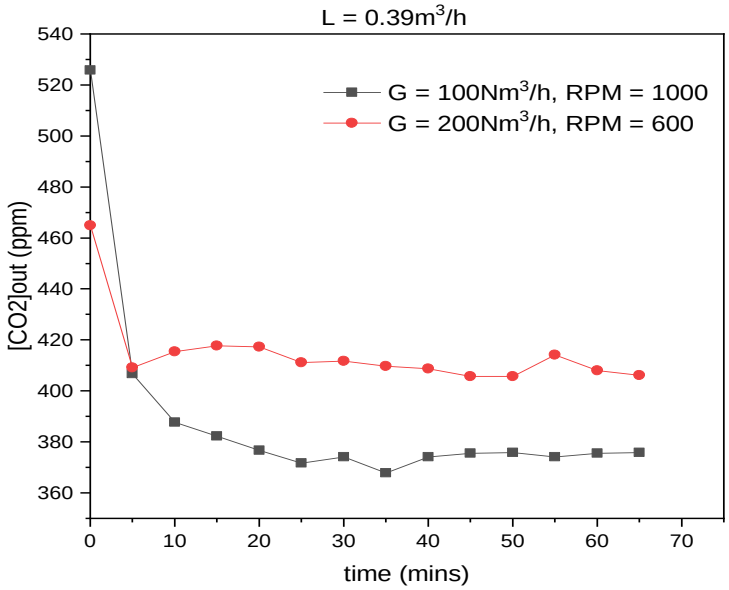

Figure 6: CO_2 concentration vs time curve for ascertaining steady state conditions

Within the investigated operating conditions, Figure 5 illustrates the stabilization of CO_2 readings after approximately an hour. Consequently, each experimental run lasted for one hour and twenty minutes to ensure measurement accuracy, with each data point being repeated at least thrice. Figure 5 also reveals that, as anticipated, under equivalent liquid flow rates, lower rotation speeds and higher gas flow rates exerted a more pronounced influence on CO_2 concentration compared to higher rotation speeds and lower gas flow rates.

3.2 Effect of Rotation Speed

In Figure 7, the impact of rotation speed, ranging from 600 to 100 rpm, on the interfacial mass transfer area at fixed gas and liquid flow rates of 100 Nm^3/h and 0.39 m^3/h, respectively is shown. The effective interfacial area ranged from 1328 to 1723 m^2/m^3, representing 55 to 77% of the geometric packing area.

This variation from the geometric and wetted areas of packings as was previously observed by Hegely et al. [7] for CPSCs, is attributed to factors such as liquid stagnation, localized saturations, and liquid flows along the contactor wall. Figure 6 also demonstrates a positive correlation between rotational speed and interfacial mass transfer area. The observed higher error bars are attributable to rapid CO_2 fluctuations. Increased rotational speeds enhance liquid dispersion and result in a larger gas-liquid contacting area, as noted by Luo et al. [8], [18]

3.3 Effect of Gas Flow Rate

The effect of gas flow rate on the interfacial area was studied at a rotation speed of 700 rpm and two liquid flow rates: 0.30 m^3/h and 0.39 m^3/h, for gas flow rates ranging from 100 to 300 Nm^3/h, as shown in Figure 8. The results indicate a direct relationship between gas flow rate and interfacial area.

Figure 7 shows that for a constant rotation speed of 700 rpm, at constant liquid flow rates of 0.30m^3/h and 0.39m^3/h respectively, the effective interfacial area improved from 1220 m^2/m^3 to 2116 m^2/m^3 and 1481 m^2/m^3 to 2325 m^2/m^3 respectively with increased gas volumetric flow from 100 to 300Nm^3/h. Within the range of operating parameters investigated, the interfacial was found to be 1220 to 2325m^2/m^3, a coverage of 51 to 97% of the geometric packing area. Increased gas flow rate leads to an increase in the gas fluxes in the packing. With increasing gas flow rate, the effective interfacial area expanded due to enhanced gas fluxes, which disrupted gas-liquid interactions and increased the gas-liquid

interface. The increase in the gas volumetric flow rate and radial velocity results in a more substantial disturbance of the gas and liquid phases, a better dispersion of the liquid, and an increase of the gas-liquid interface, which increases the effective interfacial area as was reported by Yang et al.[11]. Hence, compared to what was reported by previous seminal research conducted with stainless-steel wire-mesh packing in RPBs equipped with single gas inlets, the packing utilization factor obtained in this study exceeded what was reported by [19], [11] and [20] with 16, 27 and 33% respectively.

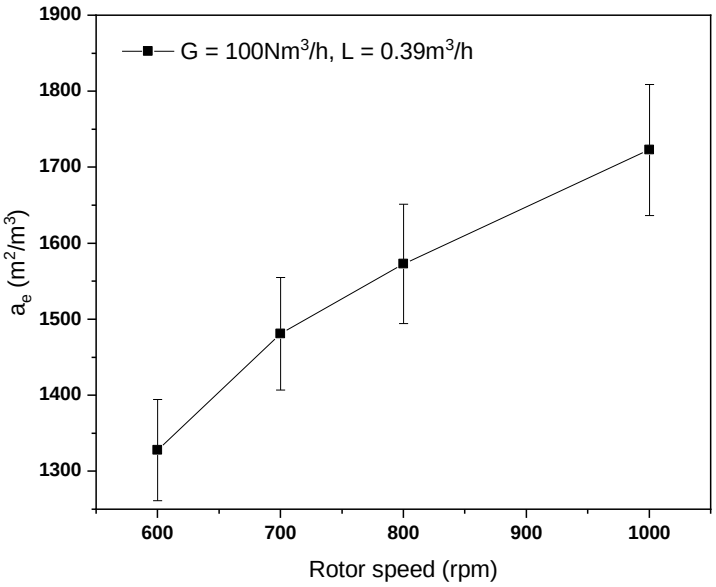

Figure 7: Effect of the rotational speed on the Interfacial mass transfer area

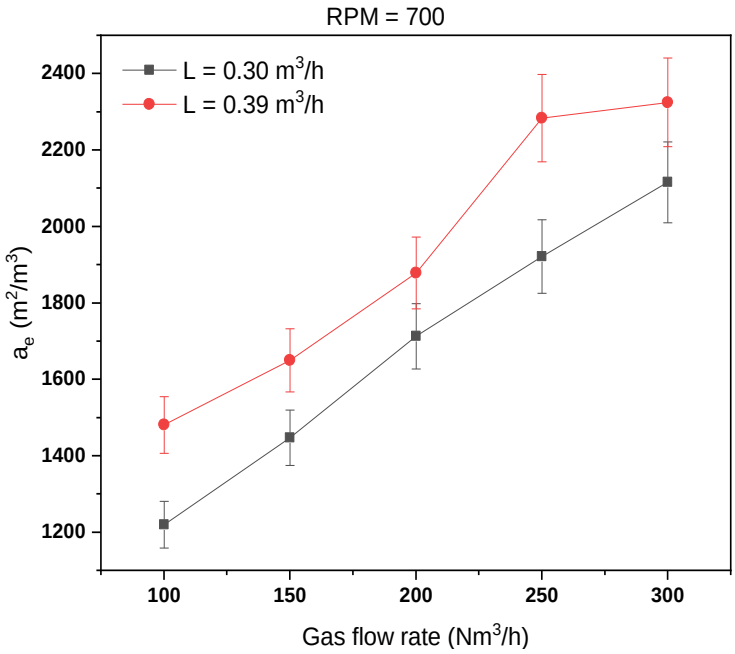

Figure 8: Effect of gas flow rate on the Interfacial mass transfer area

3.4 Effect of Liquid Flow Rate

Figure 9 shows the effect of liquid flow rate, ranging from 0.3 m^3/h to 0.6 m^3/h, on the effective interfacial area at a constant rotation speed of 700 rpm and two gas flow levels: 100 Nm^3/h and 200 Nm^3/h.

Figure 9 shows that within the experimental range, for constant gas flow rates of 100 Nm^3/h and 200Nm^3/h, the effective interfacial area increased from 1220 m^2/m^3 to 1770 m^2/m^3 and from 1713 m^2/m^3 to 1984 m^2/m^3 respectively. Hence, the results showed that within the operating parameters investigated, the interfacial area represented about 51 to 74% and 71 to

83% of the geometric packing area for a constant rotation of 700 rpm. The increased effective interfacial area increase with increased liquid flow within the experimental range is attributed to the generation of more liquid droplets, rivulets, and thin films at higher liquid flow rates.

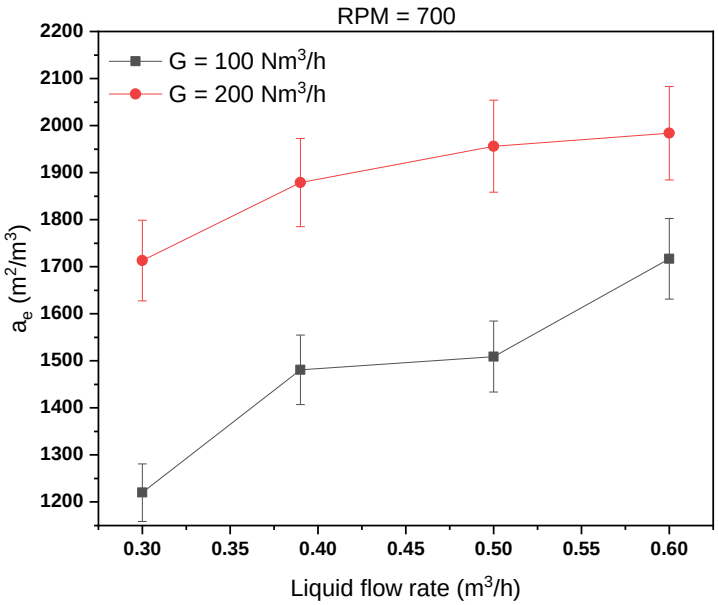

Figure 9 Effect of liquid flow rate on the Interfacial mass transfer area

3.5 Comparing the Calculated, Experimental, and Literature-Reported Effective Interfacial Area

The calculated a_e values as obtained using Equation (25) were compared with the experimentally obtained values. The initial data for this work was presented in Garba [21]. The results showed good agreement between the experimental and calculated values to within an average of 8%. Table 2 highlights a comparison of the effective interfacial area as obtained using single-gas-inlet-RPBs operated under varying operating conditions and rotor sizes as reported in the literature with what was obtained in this study using the RPB500 equipped with dual gas inlets. The packing utilization ratio, a_e/a_t compares the section of the packing utilized for the gas-liquid contact to the total surface area of the packing. The a_e/a_t obtained in this study showed higher values compare d to seminal studies conducted with single-gas-inlet RPBs. The higher a_e/a_t for the dual-gas-inlet RPB, is attributed to the relatively higher liquid holding capacity of the packing under a given centrifugal force as balanced with the more sufficient gas as introduced from opposite directions

4. CONCLUSION

This study presents experimental measurements of the effective interfacial mass transfer area of a stainless-steel strand wire-mesh packing using the CO_2-NaOH chemisorption method. Utilizing a novel pilot-scale countercurrent RPB500 equipped with two gas inlets, the research investigates the effects of rotation speed, gas, and liquid flow rates on the interfacial area. Rotation speed and gas flow rate notably influence the interfacial area, while the effect of liquid flow rate was comparatively minor. The effective interfacial area of the stainless-steel wire mesh packing was about 55 to 97% of the packing geometric packing area. Compared to what was reported for RPBs equipped with single gas inlets, the packing utilization factor obtained in this study was about 33% higher. The findings highlight increased liquid dispersion and rapid renewal of the gas-liquid contact surface as key contributors to interfacial area enhancement. Hence, compared to conventional RPBs with single-gas inlets, RPBs equipped with dual-gas inlets offer broader surfaces for mass transfer, potentially enhancing device utilization for separation purposes.

Table 2 Comparing the packing utilization factor $\left(\frac{a_e}{a_t}\right)$ values for single and dual-gas inlet RPBs

Reference	RPB, dimensions: $r_o/r_i/z$ (mm)	System	Operating Conditions	Packing Characteristics Type/a_t(m^2/m^3)/ε (%)	$\frac{a_e}{a_t}$
Jassim et al. [22]	Countercurrent 199/78/25	CO_2 in air-ethanolamine	L = 167.1 L/h RPM = 500 rpm	Stainless perspex sheets\ 2132\76	0.7298
Yang *et al.* [11]	Countercurrent (Single gas inlet)	NaOH solution-CO_2	L = 180-600L/h G = 10-40m^3/h RPM = 600-1400 rpm	Stainless steel wire mesh\ 499.7\97%	0.3804-0.7007
Luo *et al.* [18]	Countercurrent (Single gas inlet) 153/78/50	NaOH solution-CO_2	L = 100L/h G = 6 m^3/h RPM = 600-1400 rpm	Stainless steel wire mesh\400, 450, 500, 570\96	0.5807-0.8178
Mei-ying *et al.* [23]	Cross-flow (Single gas inlet) (187.5/95/176)	NaOH solution-CO_2	L = 1.1 - 2.22m^3/h G = 100 - 600m^3/h RPM = 400 -1200	RS wire mesh\780\95	0.6410- 4.4871
Chen *et al.* [24]	Countercurrent (Single gas inlet) 82/40/15	NaOH solution-CO_2	L = 0.024 m^3/h G = 1.2 m^3/h RPM = 500 -2500	Stainless wire mesh\1860\-	[24][24][24]0.4838-0.5376
Sheng *et al.* [9]	Countercurrent (Single gas inlet) 150/50/53	NaOH solution-CO_2	L=0.01-0.055L/h G = 3.5 m^3/h RPM = 600-1400	stainless wire mesh \ 1533\94	0.2600−0.6400
Tian *et al.* [4]	Countercurrent (Single gas inlet) 45-72/15.5/25-40	NaOH solution-CO_2	L = 50–300 ml^3min^{-1} G = 26 $Lmin^{-1}$ High gravity factor = 12-125	stainless steel plates with wire fillers\ 320\-	0.08-0.5900
This study	Countercurrent (Dual gas inlet) 250/80/40	NaOH solution-CO_2	L = 0.30-0.60m^3/h **G** = 100-300Nm^3/h RPM = 600-1000	stainless wire mesh \ 2400\86	0.5500-0.9700

REFERENCES

[1] Alatyar, A. M. & Berrouk, A. S. (2023). Hydrodynamic Behavior of Liquid Flow in a Rotating Packed Bed, *Chem. Eng. Res. Des*, 197(1), 851–870. www.https//:doi:10.1016/j.cherd.2023.08.032

[2] Joel, A.S., Aliyu, U.F., A. S., Olubajo, O.O. & Isa, Y.M. (2024). Performance Study on Mixed Solvent for Post-Combustion Carbon Capture using Rotating Packed Bed Technology, *Greenhouse. Gas. Sci. Technol*., 14, 400–410. www.https//:doi:10.1002/ghg.2280

[3] Shukla, C., Mishra, P. & Dash, S. K. (2023). A Review of Process Intensified CO_2 capture in RPB for Sustainability and Contribution to Industrial Net Zero, Front. Energy Res, 11, 1135188. www.https//:doi:10.3389/fenrg.2023.1135188.

[4] Tian, W., Ji, J., Li, H., Liu, C., Song, L., Ma, K., Tang, S., Zhong, S., Yue, H. & Lianget, B. (2022). Measurements of the Effective Mass Transfer Areas for the Gas–Liquid Rotating Packed Bed, *Chinese J. Chem. Eng*., 55, 13-19. www.https//:doi:10.1016/j.cjche.2022.06.002.

[5] Ghadyanlou, F., Azari, A, &. Vatani, A. (2021). A Review of Modeling Rotating Packed Beds and Improving Their Parameters: Gas–Liquid Contact. *Sustainability*, 13, 8046. https://doi.org/10.3390/su13148046

[6] Nugroho, M. A., Susanto, Y. B., Kamilah, V. L. & Prameswari, R. (2023). Carbon Dioxide (CO_2) Absorption Process using Sodium Hydroxide (NaOH), *IPTEK J. Eng*., 9(1), 30. https://doi:10.12962/j23378557.v9i1.a15192

[7] Hegely, L., Roesler, J., Alix, P., Rouzineau, D. & Meyer, M. (2017). Absorption methods for the Determination of Mass Transfer Parameters of Packing Internals: A Literature Review, *AIChE J*. 63(8), 246–3275. https://doi:10.1002/aic.15737.

[8] Luo, Y., Luo, J. Z., Chu, G. W., Zhao, Z. Q., Arowo, M. & Chen, J. F. (2017). Investigation of Effective Interfacial Area in a Rotating Packed Bed with Structured Stainless Steel Wire Mesh Packing, Chem. *Eng. Sci.*, 170, 347–354. https://doi:10.1016/j.ces.2016.10.023.

[9] Sheng M., Xie,C., Sun, B., Luo, Y., Zhang, L.J., Chu,G., Zou, H. & Chen, J. F. (2019). Effective Mass Transfer Area Measurement Using a CO_2-NaOH System: Impact of Different Sources of Kinetics Models and Physical Properties, *Ind. Eng. Chem. Res*, 58(25), 11082–11092. https://doi:10.1021/acs.iecr.9b00538.

[10] Neumann, K., Hunold, S., Beer, M. D., Skiborowski, M. & Górak, A. (2018). Mass Transfer Studies in a Pilot Scale RPB with Different Packing Diameters, *Ind. Eng. Chem. Res*, 57(6), 2258–2266. https://doi:10.1021/acs.iecr.7b04186.

[11] Yang, K., Chu, G., Zou, H., Sun, B., Shao, L. & Chen, J.F. (2011). Determination of the Effective Interfacial Area in Rotating Packed Bed, *Chem. Eng. J*, 168(3), 1377–1382. https://doi:10.1016/j.cej.2011.01.100.

[12] Yuan, Z. G., Wang, Y. X., Liu, Y. Z., Wang, D., Jiao, W.-Z. & Liang, P.F. (2022). Research and Development of Advanced Structured Packing in a Rotating Packed Bed, *Chinese J. Chem. Eng*, 49, 178–186. https://doi:10.1016/j.cjche.2021.12.023.

[13] Luo, Y., G Chu, G.W., Zou, H. K., Wang, F., Xiang, Y., Shao, L., & Chen, J.F. (2012). Mass Transfer Studies in a Rotating Packed Bed with Novel Rotors: Chemisorption of CO_2. *Ind. Eng. Chem. Res*, 51(26), 9164–9172, https://doi:10.1021/ie300466f.

[14] Wu, W., Luo, Y., Chu, G. W., Su, M. J., Cai, Y., Zou, H. K. & Chen, J. F. (2020). Liquid Flow Behavior in a Multiliquid-Inlet Rotating Packed Bed Reactor with Three-Dimensional Printed Packing. *Chemical Engineering Journal*, 386. https://doi.org/10.1016/j.cej.2019.04.117.

[15] Elcner, J. & Jicha, M. (2020). Effect of Multiple Liquid Inlets on Mass Transfer in Rotating Packed Beds, *MATEC Web Conf.*, 328, 02010. https://doi:10.1051/matecconf/202032802010.

[16] Gładyszewski, K., Grob, K., Bieberle, A., Schubert, M., Hild, M., Górak, A. & Skiborowski, M. (2021). Evaluation of Performance Improvements Through Application of Anisotropic Foam Packings In Rotating Packed Beds, *Chemical Engineering Science* ,230. https://doi.org/10.1016/j.ces.2020.116176.

[17] Garba, U., Rouzineau, D. & Meyer, M. (2023). Study of the Hydrodynamic Performance of a Compact and Intensified G /L Contactor : the RPB," MATEC Web Conf. 379, 04003 SFGP2022,04003,1–8, https://doi.org/10.1051/matecconf/202337904003

[18] Luo, Y., Chu, G. W., Zou, H. K., Z. Q. Zhao, Dudukovic, M. P. & Chen, J. F. (2012). Gas-Liquid Effective Interfacial Area in a Rotating Packed Bed, *Ind. Eng. Chem. Res*, 51(50) 16320–16325. https://doi:10.1021/ie302531j.

[19] Guo, K., Zhang, Z., Luo, H., Dang, J. & Qian, Z. (2014). An Innovative Approach of the Effective Mass Transfer Area in the Rotating Packed Bed, *Ind. Eng. Chem. Res*, 53 (10), 4052–4058. https://doi:10.1021/ie4029285.

[20] Sheng, M., Xie, C., Zeng, X., Sun, B., Zhang, L., Chu, G., Luo, L., , Chen, J.F. & Zou, H. (2018). Intensification of CO_2 Capture using Aqueous Diethylenetriamine (DETA) Solution from Simulated Flue Gas in a Rotating Packed Bed, *Fuel*, 234(15), 1518–1527. https://doi:10.1016/j.fuel.2018.07.136.

[21] Garba, U. (2023). Study of the Impact of the Morphology of a G/L Contactor on the Hydrodynamics and Mass Transfer in an RPB : Application to the Treatment of Gases in an Embedded Process, PhD Thesis, University of Toulouse, France. https://theses.hal.science/tel-04163687/

[22] Jassim, M. S., Rochelle, G., Eimer, D. & Ramshaw, C. (2007). Carbon Dioxide Absorption and Desorption in Aqueous Monoethanolamine Solutions in a Rotating Packed Bed, *Ind. Eng. Chem. Res*, 46(9), 2823–2833. https://doi:10.1021/ie051104r.

[23] Mei-ying, W. T., Gui-sheng, D., You-zhi, Q., Qiang, L. & Song Bin, G. (2015). Experimental Study on Influential Factors of Mass Transfer in a Cross-Flow Rotating Packed Bed [In Chinese], *Chin. J. Process Eng*, 15(6), 929–934.
[24] Chen, Q. Y., Chu, G. W., Luo, Y., Sang, L., Zhang, L.L., Zou, H. K. & Chen, J. F. (2016). Polytetrafluoroethylene Wire Mesh Packing in a Rotating Packed Bed: Mass-Transfer Studies, *Ind. Eng. Chem. Res*, 55(44), 11606–11613. https://doi:10.1021/acs.iecr.6b02630.